JOURNAL OF GEOPHYSICAL RESEARCH, VOL. 106, NO. D22, PAGES 28,555–28,566, NOVEMBER 27, 2001

Column-integrated aerosol optical properties over the Maldives during the northeast monsoon for 1998–2000

T. F. Eck,[1] B. N. Holben,[2] O. Dubovik,[3] A. Smirnov,[3]
I. Slutsker,[3] J. M. Lobert,[4] and V. Ramanathan[4]

Abstract. Measurements made during the Indian Ocean Experiment (INDOEX) have shown the presence of large aerosol loadings over the region of the northern Indian Ocean and Arabian Sea. In recent years there has been significant interannual variability in the magnitude of this aerosol loading during the NE monsoon months of January–April. Monitoring of the integrated atmospheric column effective aerosol optical properties was initiated in early 1998 and continued in 2000 on the island of Kaashidhoo in the Republic of Maldives. An Aerosol Robotic Network Sun-sky radiometer at the Kaashidhoo Climate Observatory made spectral measurements of the direct Sun and directional sky radiances which were utilized to infer spectral aerosol optical depths τ_a, single scattering albedos, asymmetry factors, and aerosol size distributions. Monthly average aerosol optical depths at 500 nm varied by more than a factor of 2 during January through April for the 3 years that were investigated, 1998–2000. Interannual variations in the monthly mean Angstrom wavelength exponent were also observed, resulting from differences in the bimodal aerosol size distributions. Spectral variations in the Angstrom wavelength exponent were observed, especially at high aerosol optical depths when fine mode aerosols dominated over the optical influence of coarse-mode aerosols. Some differences in spectral single scattering albedo and asymmetry factor were observed for 1999 versus 2000 in the infrared wavelengths, but with relatively little change in the visible wavelengths. The spectral variation in the retrieved single scattering albedo was large, with approximately linear wavelength dependence averaging from 0.91 at 440 nm to 0.83 at 1020 nm for January–March 1999 for observations where τ_a at 440 nm >0.4.

1. Introduction

Radiative forcing due to atmospheric aerosols is one of the largest sources of uncertainty in assessing future climate change [*Hansen et al*., 2000]. Depending on the magnitude of the aerosol absorption, the aerosols may either counter or enhance the warming influence of globally increasing greenhouse gases. This can occur through direct radiative forcing, indirect radiative forcing by modification of cloud optical properties and/or lifetimes, and "semidirect forcing" [*Hansen et al*., 1997] from the effects of increasing atmospheric heating in the aerosol layer and thereby evaporating clouds and/or suppressing convection.

The INDOEX experiment [*Ramanathan et al*., this issue] was conducted from 1997–1999 mainly over the Arabian Sea and Indian Ocean (principally in the Northern Hemisphere) to study the effects of anthropogenic atmospheric pollutants and natural emissions (aerosols and gases) on the radiative energy balance and climate of the region. Analysis by *Satheesh and Ramanathan* [2000] of data acquired during INDOEX has shown that the absorbing aerosols present over the northern Indian Ocean (Maldives Islands) in the winter northeast (NE) monsoon resulted in a threefold difference between the direct (cloudless sky) radiative heating at the top of the atmosphere and the ocean surface. This aerosol radiative forcing may have implications for a slowing of the hydrological cycle. In addition, modeling studies of aerosol layer heating induced by soot absorption in the INDOEX study region have shown a resultant reduction in daytime low-altitude cloud cover [*Ackerman et al*., 2000] which may offset some of the aerosol cooling effect (due to scattering) and further modify the hydrological cycle. Regional distributions of aerosols [*Rajeev et al*., 2000], interannual variability of aerosol concentrations, and detailed descriptions of spectral aerosol optical properties are needed in order to more fully understand the influences of aerosols on the climate of the region. In particular, there have not been any measurements yet reported on the spectral variation of aerosol absorption for the region or of the spectral variation in aerosol scattering phase function. Detailed information on the spectral variation of aerosol absorption is very important as estimates by *Hansen et al*. [2000] suggest that black carbon aerosols contribute significantly to global warming.

In conjunction with the INDOEX experiment field experiment activity, NASA's Aerosol Robotic Network (AERONET) project

[1]Goddard Earth Sciences and Technology Center, University of Maryland-Baltimore County, NASA Goddard Space Flight Center, Greenbelt, Maryland, USA.
[2]Biospheric Sciences Branch, NASA Goddard Space Flight Center, Greenbelt, Maryland, USA.
[3]Science Systems and Applications Inc., NASA Goddard Space Flight Center, Greenbelt, Maryland, USA.
[4]Center for Clouds, Chemistry, and Climate, Scripps Institution of Oceanography, University of California, San Diego, La Jolla, California, USA.

Paper number 2001JD000786.
0148-0227/01/2001JD000786$09.00

[*Holben et al*., 1998] installed a CIMEL Sun-sky radiometer in the Maldives on the island of Kaashidhoo in late 1997. AERONET currently continues to operate and maintain a CIMEL radiometer in the Maldives, with a plan for long-term aerosol optical properties monitoring in the region. In this paper we present results of the analysis of these data from February 1998 through May 2000, focusing most of our analysis on the peak NE monsoon dry season months of January–April. The total atmospheric column-integrated aerosol optical properties, derived from both direct Sun and sky radiance measurements, of spectral optical depth, single scattering albedo, size distribution, and asymmetry factors are presented. We present data on the interannual variability of these parameters but place more emphasis on the January–March 1999 period since this was the time when the largest number of field investigations were performed within the intensive field phase of INDOEX.

2. Instrumentation and Methodology

The measurements presented in this paper were made on the island of Kaashidhoo in the Maldives, approximately 500 km southwest of the southern tip of India. Kaashidhoo is a small island, ~3 km by ~1 km, with a population of ~1600. The CIMEL Electronique CE-318 Sun-sky radiometer measurements taken at the Kaashidhoo Climate Observatory (KCO) at 4.966°N, 73.466°E (on the top of a 13.1 m tower) were made with instruments that are a part of the AERONET global network. The CIMEL radiometers and the satellite transmitters, which operate within the AERONET network, are powered by batteries charged from solar photovoltaic panels, without dependency on the local power supply. This independent operating mode enabled the uninterrupted collection of data at KCO even during a period of intermittent AC power supply to KCO in the late winter-spring of 2000. The CIMEL radiometers are described in detail by *Holben et al*. [1998]; however, a brief description will be given here. The automatic tracking Sun and sky scanning radiometers made direct Sun measurements with a 1.2° full field of view every 15 min at 340, 380, 440, 500, 675, 870, 940, and 1020 nm (nominal wavelengths). The direct Sun measurements take ~8 s to scan all eight wavelengths, with a motor-driven filter wheel positioning each filter in front of the detector. These solar extinction measurements are then used to compute aerosol optical depth at each wavelength except for the 940 nm channel, which is used to retrieve total column water vapor in centimeters. The filters utilized in these instruments were ion-assisted deposition interference filters with band pass (full width at half maximum) of the 340 nm channel at 2 nm and the 380 nm filter at 4 nm, while the band pass of all other channels was 10 nm. The CIMEL radiometer at KCO was exchanged with a freshly calibrated unit approximately every 6 to 10 months for the 1998–2000 time period.

Calibration of the field instruments was performed by a transfer of calibration from reference instruments which were calibrated by the Langley plot technique at Mauna Loa Observatory (MLO), Hawaii. Reference instruments are typically calibrated at MLO every 2–3 months using morning measurements only. The intercalibration of field instruments was performed both predeployment and postdeployment at Goddard Space Flight Center (GSFC), and a linear change in calibration with time was assumed in the interpolation between the two calibrations. The combined effects of uncertainties in calibration, atmospheric pressure (not monitored), and total ozone amount (climatology is used) result in a total uncertainty of ~0.010–0.021 in computed τ_a for field instruments (which is spectrally dependent with the higher errors in the UV [*Eck et al*., 1999]). *Schmid et al*. [1999] compared τ_a values derived from four different solar radiometers (one was an AERONET Sun-sky radiometer) operating simultaneously together in a field experiment and found that the τ_a values from 380 to 1020 nm agreed to within 0.015 (RMS), which is similar to our estimated level of uncertainty in τ_a retrieval for field instruments.

Total column water vapor is retrieved primarily from the 940 nm direct Sun measurements utilizing the technique of *Bruegge et al*. [1992]. Given that the current estimates of water vapor absorption magnitude in this spectral region has changed significantly in recent years, and the relatively large uncertainty in modified Langley zero air mass voltage at 940 nm, we conservatively estimate our uncertainty in column water vapor amount to be ~10%.

The CIMEL sky radiance almucantar measurements at 440, 675, 870, and 1020 nm in conjunction with the direct Sun measured τ_a at these same wavelengths were used to retrieve aerosol size distributions following the methodology of *Dubovik and King* [2000]. Almucantar sky radiance measurements were made at optical air masses of 4, 3, and 2 in the morning and afternoon, and once per hour in between. Spherical particle shape is assumed in the retrievals, which is typical for biomass burning aerosols [*Martins et al*., 1998], and also for hygroscopic aerosols such as sulfates or sea salt. Transmission electron microscope images of INDOEX study region particles from north of the Intertropical Convergence Zone [*Ramanathan et al*., this issue] suggest that many are close to spherical in shape. Desert dust aerosols often exhibit a significant degree of nonsphericity, and the retrieval assumption of spherical particle shape in this case results in an overestimation of the volume of fine-mode particles [*Dubovik et al*., 2000]. Sensitivity studies performed by *Dubovik et al*. [2000] were used to analyze the perturbations of the inversion resulting from random errors, possible instrument offsets, and known uncertainties in the atmospheric radiation model. Retrieval tests using known size distributions demonstrated successful retrievals of mode radii and the relative magnitude of modes for various types of size distributions such as bimodal accumulation mode dominated aerosols and bimodal coarse-mode-dominated aerosols. Simultaneous retrievals of aerosol single scattering albedo are also made with this algorithm, and the sensitivity analysis shows that these retrievals have an uncertainty of ~0.03 when aerosol optical depth at 440 nm is >0.5 [*Dubovik et al*., 2000].

3. Aerosol Physical and Radiative Properties

The analyses that we present from measurements of spectral direct Sun and sky radiances are representative of the aerosol optical properties integrated over the entire atmospheric column from the surface (ocean) to the top of the atmosphere. Therefore some of these parameters, such as the single scattering albedo, the size distribution, and the asymmetry parameter, are the radiatively effective column-integrated values. As a result, they may differ from either surface-based in situ air sampling measurements or from similar in situ types of measurements made at specific altitudes from aircraft since the aerosol may at times be composed of somewhat distinct vertical layers. These layers contain aerosols that may originate

from different source regions. As an example, analysis by *Lobert and Harris* [in press] show that for March 1999 the 10-day trajectories arriving at KCO at 500 m altitude are from Arabia and the Arabian Sea, while at 1500 and 2500 m above sea level the air masses arrive from the Bay of Bengal and India. Aerosols originating from such differing source regions are likely to have significant differences in their optical properties. However, the column-integrated values of the parameters which we provide are nonetheless very useful in the analysis and retrieval of aerosol properties from satellite remote sensing measurements [*King et al*., 1999] and in the analysis of the radiative forcing effects which these aerosols exert on the regional climate.

3.1. Aerosol Optical Depth

We focus our analysis primarily on the winter monsoon months of January–April when the flow is primarily from the northeast from the Indian subcontinent, and also from southern Asia and Arabia. This was also the time period of primary emphasis for the INDOEX field experiment campaigns in 1998 and 1999, when extensive measurements were made from land, ships, and aircraft. In addition, we include the transition months of May and June in some of our analyses, when the large-scale circulation pattern is shifting to a southwest monsoon, with air masses originating over the relatively unpolluted southern Indian Ocean.

Figure 1 shows the January through June monthly average aerosol optical depth at 500 nm (τ_{a500}) at KCO for 3 years, 1998–2000, with error bars depicting one standard deviation of the daily average τ_{a500} values. These data have been screened for clouds, following the methodology of *Smirnov et al*. [2000]. This technique relies on the greater temporal variance of cloud optical depth versus aerosol optical depth, therefore temporally and spatially uniform cloud may at times be misidentified as cloud-free. There are no data shown for January 1998 since monitoring started on February 20, 1998, at KCO, and there are no data shown for June 2000 since the CIMEL radiometer was switched on May 24, 2000, and the final reprocessed and calibrated data are not yet available. Significant interannual variability in τ_{a500} is noted in Figure 1, with monthly average values in February through April 1999 more than double those measured in 1998, and with the year 2000 values intermediate in magnitude. With the transition to and onset of the SW monsoon in May and June, the monthly average τ_{a500} drops significantly in 1999 and 2000, while in 1998 the τ_{a500} in May–June are similar to values in the peak NE monsoon months. For the transition month of May all 3 years show nearly equal τ_{a500} values, and the years 1998 and 1999 also show nearly equal values in June. However, the trajectories in June 1999 were mainly from the southern Indian Ocean, while in June 1998 there was a mixture of trajectories from the Horn of Africa region and Madagascar and from the southern Indian Ocean. In contrast, large interannual variability in τ_{a500} for the peak NE monsoon months of February through April suggest large year-to-year variability in the source strengths, and/or trajectories and/or large-scale circulation. Trajectory analyses for KCO by *Lobert and Harris* [this issue] show similar air mass source regions in March for both 1998 and 1999, despite the τ_{a500} being more than 2 times greater in 1999. Therefore the reasons for the interannual differences noted in these years may be related to differences in large-scale vertical and horizontal dispersion which may result in part from differences in subsidence strength. Daily average values of τ_{a500} exhibit large day-to-day changes (Figure 2) and variable trajectories within each month, which *Lobert and Harris* [this issue] have shown for KCO are likely to be the dominant reason for this variability.

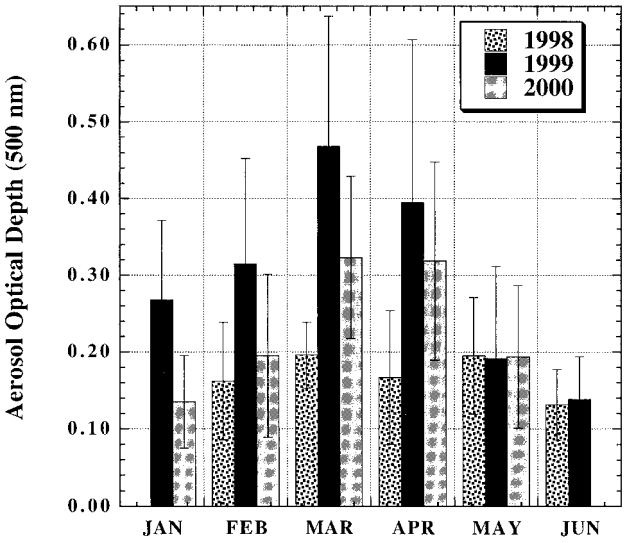

Figure 1. Monthly average τ_{a500} at the Kaashidhoo Climate Observatory (KCO) for the months January–June 1998–2000. Error bars show one standard deviation of the daily average values.

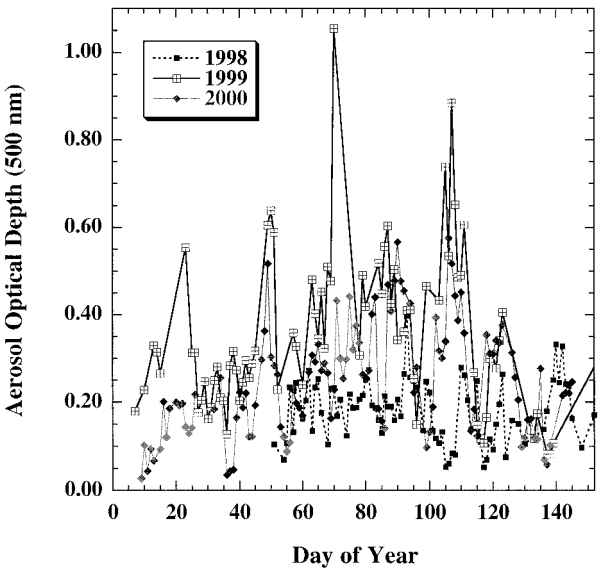

Figure 2. Time series of the daily average values of τ_{a500} for January–May 1998–2000 at KCO, depicting the large day-to-day variability due in part to variable trajectories.

The Angstrom wavelength exponent α, which is a measure of the wavelength λ dependence of τ_a and therefore sensitive to particle size distribution, can be computed from aerosol optical depth data at two wavelengths from

$$\alpha = -\frac{d \ln \tau_a}{d \ln \lambda} = -\frac{\ln\left(\frac{\tau_{a_2}}{\tau_{a_1}}\right)}{\ln\left(\frac{\lambda_2}{\lambda_1}\right)}. \quad (1)$$

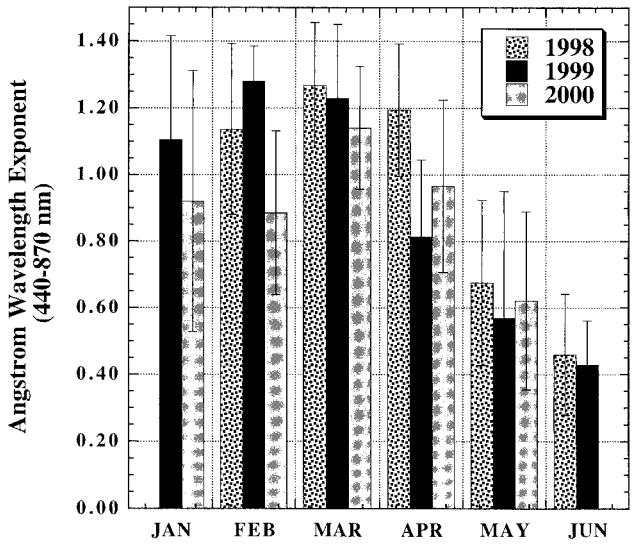

Figure 3. Monthly average Angstrom wavelength exponent α at KCO for the months January–June 1998–2000. The Angstrom wavelength exponent ($\alpha_{440-870}$) was computed from linear regression of ln τ_a versus ln λ utilizing the 440, 500, 675, and 870 nm data. Error bars show one standard deviation of the daily average values.

Size-dependent aerosol composition has a much smaller influence on α than size distribution. For fine-mode aerosols, *Eck et al.* [2001] have shown that changing the black carbon content (which modifies both the real and imaginary part of the refractive indices) has a relatively small influence on α, while for coarse-mode particles a change in refractive index has even less effect on α. Although AERONET performs aerosol size distribution retrievals from almucantar sky radiance inversions (section 3.2), relatively few almucantar sky radiance scans are made per day. For cloudless conditions there are eight almucantar scans made per day with solar zenith angle >50°, while there are ~55 direct Sun aerosol optical depth measurements made per day (at Kaashidhoo in the NE monsoon season). Additionally, more direct Sun aerosol optical depth measurements can be typically made under partially cloudy conditions when the cloud contamination may preclude almucantar retrievals. Another reason for analysis of the Angstrom wavelength exponent is that many satellite-based and ground-based measurements provide retrievals of spectral aerosol optical depth, but no direct size distribution retrievals, so analysis of α is important in the interpretation of these data and in providing further information on particle size.

Multiple wavelength values of τ_a may also be used to compute α from linear regression of instantaneous ln τ_a measurements versus ln λ, and we have utilized τ_a measurements made at 440, 500, 675, and 870 nm. Daily and monthly averages were then computed and are shown in Figure 3 with error bars depicting one standard deviation of the daily average values. The monthly and interannual variations in the Angstrom wavelength exponent (Figure 3) suggest significant variations in the aerosol particle size distributions at KCO. For example, in 1999 there is a significant drop in α from March to April, and the trajectory analyses of *Lobert and Harris* [this issue] show a marked shift in the trajectories with air masses originating in March over the Bay of Bengal, India, and the Arabian Sea but shifting westward in April to air masses originating primarily over the Arabian Sea and Arabia. Thus the lower values of α in April 1999 which are indicative of an increased coarse particle contribution are consistent with air originating over desert regions which would be a source of coarse-mode desert dust aerosols. Interannual variability in α during the NE monsoon months is noted (Figure 3), with α in January through March 2000 lower than for the same months in 1999 and 1998. Even though the magnitude of τ_{a500} is relatively constant in 1998 for the February through June period, the value of α drops significantly from ~1.2 in April 1998 to ~0.45 in June 1998. Trajectories in April 1998 for KCO [*Lobert and Harris*, this issue] show air masses originating in regions where there is pollution and therefore more dominant fine-mode particles (SE Asia, India, Arabian Sea), while in June 1998 the trajectories are from the south equatorial Indian Ocean and east coast of Africa where coarse-mode maritime aerosols (and possibly some soil dust aerosol) are more dominant.

The relationship between τ_{a440} and total column-integrated water vapor or precipitable water (PW) for January–March 1999 is shown in Figure 4. A wide range of aerosol optical depths occur for the PW range of 4–6 cm; however, there is a clear upper boundary envelope to τ_{a440}, with τ_{a440} increasing as PW increases from 2.5 to 5 cm. This may be the result of a combination of the influences of hygroscopic growth of aerosols due to relative humidity increases and due to a coupling of water vapor and aerosol characteristics for air masses from different source regions. *Satheesh et al.* [1999] found a correlation between daily mean relative humidity at the surface and total PW as determined from the CIMEL measurements for February–March 1998 with $r = 0.62$. In addition, they found from the analysis of data with low wind speeds (to eliminate wave-generated marine aerosols from the analysis) that τ_{a500} increases ~0.0083 per unit increase in RH (where RH varied from ~66 to 77% during the study period). However, it is noted that the τ_{a500} were at least a factor of 2 smaller in 1998 than in 1999 so it is possible that the hygroscopic growth in 1999 was greater in terms of magnitude of τ_{a500}.

The values of α computed from the 440, 500, 675, and 870 nm instantaneous measurements of τ_a for January–March

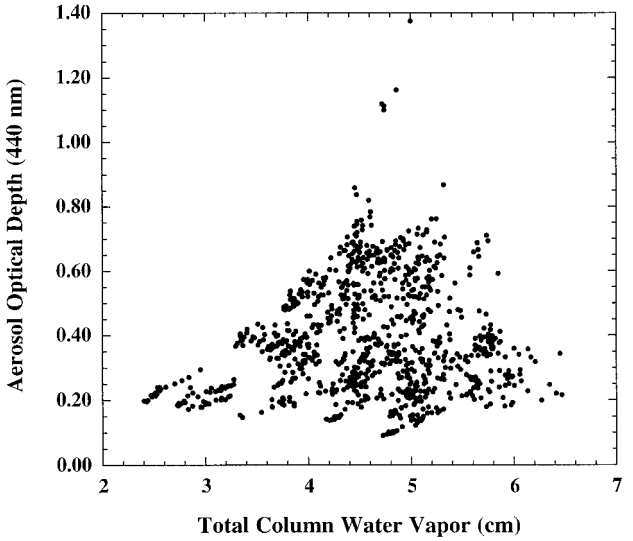

Figure 4. Instantaneous measurements of aerosol optical depth at 440 nm versus total column water vapor amount at KCO for the NE monsoon months of January–March 1999.

1999 are shown plotted versus τ_{a440} in Figure 5. There is no clear relationship between α and τ_{a440}, with most of the α observations between 1.0 and 1.55. Angstrom exponent values of this magnitude are indicative of bimodal aerosol size distributions, with significant contributions of both fine-mode submicron (radius <1 μm) and coarse-mode supermicron (radius >1 μm) aerosols [*Eck et al*., 1999; *Holben et al*., 2001]. The Angstrom wavelength exponent computed from instantaneous τ_a measurements at 340 and 440 nm (equation (1)) is shown in Figure 6. As shown by *Reid et al*. [1999], from Mie calculations utilizing measured size distributions of biomass burning aerosols in Amazonia, the Angstrom exponent at shorter wavelengths is more sensitive than at longer wavelengths to changes in particle size and width of the accumulation mode. Therefore the decrease of $\alpha_{(340-440)}$ with increasing aerosol optical depth is related to the increase in accumulation mode particle size as τ_a increases, which is also shown in Figure 6. A similar relationship to this for short wavelength α was found for biomass burning aerosols in African savanna grasslands in Zambia [*Eck et al*., 2001]. The fine-mode radius size shown in Figure 6 is determined as the maximum value of dV/d ln r of the accumulation mode size distribution (see Figure 9, section 3.2). This increase in particle size with increasing aerosol optical depth is most likely due to both aerosol hygroscopic growth and the aging processes of coagulation, condensation, and gas-to-particle conversion [*Reid et al*., 1998]. Although there is considerable scatter in the relationship between fine-mode peak radius and τ_{a440} ($r = 0.60$), the removal of one outlier point (at $\tau_{a440} \sim 0.33$) resulted in an increase of correlation coefficient r to 0.78 (61% of the variance explained). Therefore α computed from τ_a at visible to near-infrared wavelengths can be utilized to provide information on the relative influence of coarse versus accumulation mode aerosols, while α at ultraviolet to visible wavelengths is much more sensitive to the size of the accumulation mode aerosols with much less influence of the coarse mode [see also *O'Neill et al*., 2001].

For fine-mode-dominated aerosols at high aerosol optical depths a second-order polynomial fit to the ln τ_a versus ln λ data provides excellent agreement with measured τ_a, resulting in differences on the order of the uncertainty in the measurements ($\sim$0.01), while a linear fit of ln τ_a versus ln λ (α) yields significant differences with measured τ_a [*Eck et al*., 1999]. For example, measurements made at KCO on February 19, 1999, at 0452 UT, when $\tau_{a500} = 0.63$, are shown in Figure 7. The second-order fit (to the 340 to 870 nm data) for this case resulted in agreement with measured τ_a values ranging from 0.001–0.008 from 340 to 870 nm, while the linear fit resulted in differences of ~ -0.06 at 340 nm and $\sim$0.04 at 500 nm. We did not fit the second-order polynomial with the 1020 nm τ_a included, since there are possible water vapor absorption effects at that wavelength which we do not subtract in our computation of aerosol optical depth. *Shaw* [1980] reported anomalous weak absorption at 1010 nm from measurements at Mauna Loa Observatory, Hawaii, and suggested that the absorber may have been water vapor since the extinction at this wavelength increased when column water vapor increased. Computations of water vapor transmittance for the band pass of our 1020 nm filters, using a line-by-line model [*Clough et al*., 1992] and the most recent water vapor line spectrographic parameters as given by *Giver et al*. [2000], resulted in a computed water vapor optical depth of $\sim$0.009 for a tropical atmosphere with 4.0 cm of PW. This is approximately half of the measured versus computed difference of 0.02, using the second-order fit from 340 to 870 nm τ_a data, where PW = 4.5 cm for this observation date and time. It is also noted that the uncertainty of the τ_a retrieval for 1020 nm is greater than for the other non-UV wavelengths since the CIMEL silicon detector is temperature-sensitive at that wavelength ($\sim$0.25%/°C). Although the temperature of the CIMEL sensor head is monitored and a correction is applied to the measured signal to account for this dependence, this remains a source of τ_a uncertainty at 1020 nm that does not exist for the other wavelengths where the detector temperature sensitivity is insignificant.

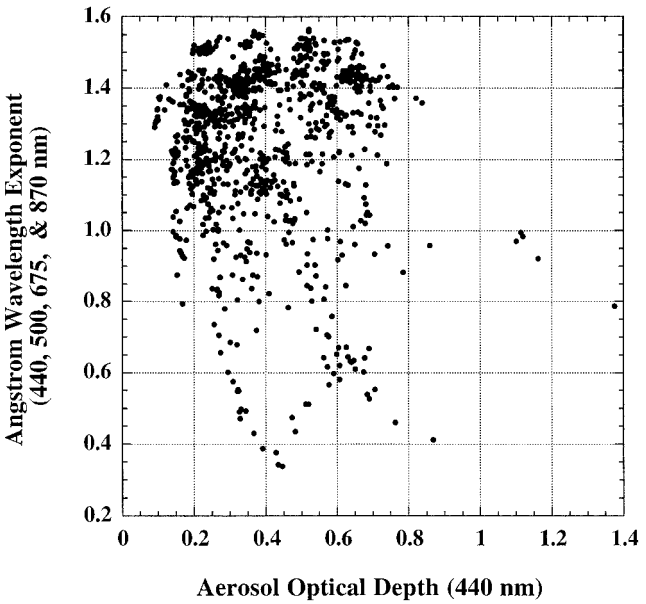

Figure 5. Instantaneous measurements of $\alpha_{440-870}$ versus aerosol optical depth at 440 nm at KCO for the NE monsoon months of January–March 1999.

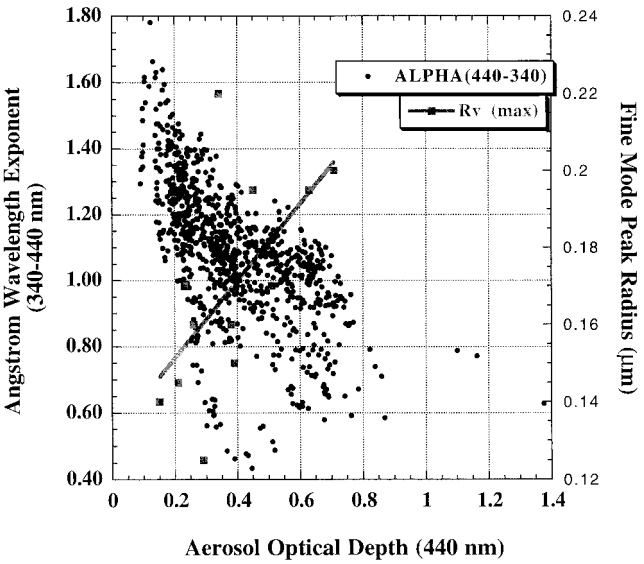

Figure 6. The Angstrom wavelength exponent computed from the 340 and 440 nm wavelength pair using equation (1) versus aerosol optical depth at 440 nm. Also shown is the radius of the fine-mode peak value of dV/d ln r for KCO, determined from the data shown in Figure 9.

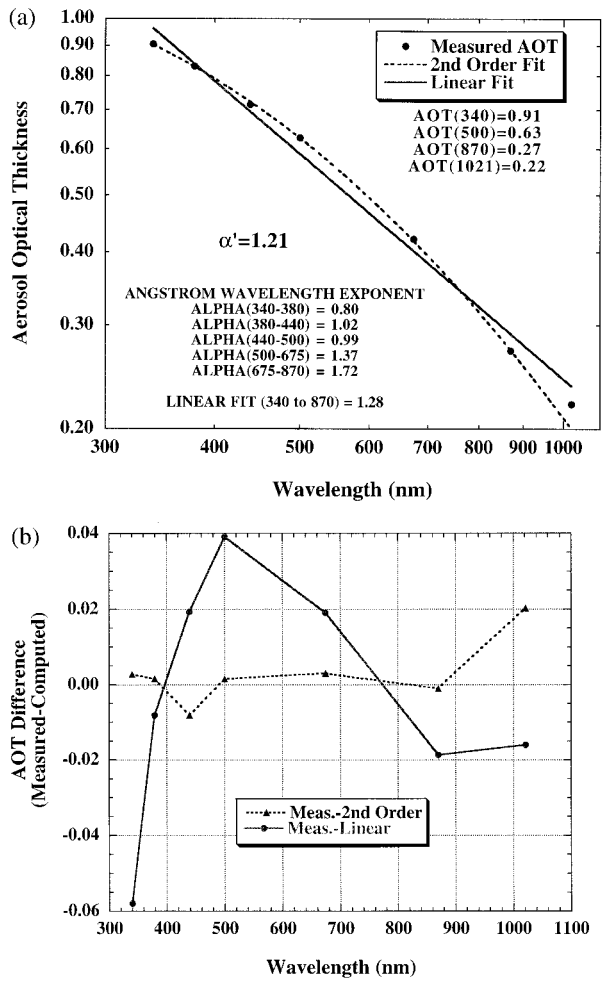

Figure 7. (a) The spectral variation of measured τ_a (340–1020 nm) from the AERONET CIMEL radiometer at KCO on February 19, 1999, at 0452 UT. The linear fit and the second-order polynomial fit of ln τ_a versus ln λ to the measurements are also shown. The aerosol optical thickness (AOT) for this case at 500 nm was 0.63. (b) The difference between the measured τ_a (shown in Figure 7a) and the value obtained from the linear and second-order polynomial fits at the measurement wavelengths.

As a parameter to quantify the curvature of the ln τ_a versus ln λ relationship, we utilize the second derivative of ln τ_a versus ln λ, or the derivative of α with respect to the logarithm of wavelength [*Eck et al.*, 1999]. The second derivative is a measure of the rate of change of the slope with respect to wavelength and therefore is a complement to the Angstrom exponent, which is the negative of the slope (first derivative) of ln τ_a versus ln λ. We use the following approximation to compute the second derivative, and we define $\alpha'(\lambda_i)$ at wavelength λ as the negative of the second derivative (since α is defined as the negative of the first derivative):

$$\alpha'(\lambda_i) = \frac{d\alpha}{d \ln \lambda} = -\left(\frac{2}{\ln \lambda_{i+1} - \ln \lambda_{i-1}}\right)\left[\frac{\ln \tau_{a_{i+1}} - \ln \tau_{a_i}}{\ln \lambda_{i+1} - \ln \lambda_i} - \frac{\ln \tau_{a_i} - \ln \tau_{a_{i-1}}}{\ln \lambda_i - \ln \lambda_{i-1}}\right]. \quad (2)$$

The values of α' for KCO, computed from the 380, 500, and 870 nm τ_a, are shown in Figure 8 as a function of τ_{a440} for the same data set as was used in Figures 5 and 6. Large positive values of α' are characteristic of fine-mode-dominated aerosol size distributions [*Eck et al.*, 1999], which were also observed for biomass burning aerosols in Amazonia and Africa, while near-zero and negative values of α' are characteristic of size distributions with a dominant coarse mode or bimodal distributions with a coarse mode having a significant relative magnitude [*Eck et al.*, 1999; *O'Neill et al.*, 2001]. There is a tendency toward larger values of α' as τ_{a440} increases due to a stronger optical influence of fine-mode particles at the higher optical depths, which are often the result of pollution transport from India and southern Asia. For cases where α' is positive a linear (Angstrom) fit of ln τ_a versus ln λ for all wavelengths will result in the linear fit overestimating τ_a at the lowest and highest wavelengths and underestimating τ_a at the middle wavelengths.

3.2. Aerosol Size Distributions

The retrieved aerosol volume size distributions for the aerosols over KCO from January–March 1999 are shown in Figure 9. These size distributions were derived from the algorithm of *Dubovik and King* [2000], which utilized measurements of spectral τ_a and almucantar sky radiance distributions at 440, 675, 870, and 1020 nm (for observations when solar zenith angle >54°) from a CIMEL Sun-sky radiometer. The aerosol size distributions presented are effective total atmospheric column-integrated size distributions that are consistent with the column-integrated radiative effects of the aerosols. As is seen in Figure 9, the accumulation mode particles (<0.6 μm) are nearly lognormally distributed. Lognormal distributions are often utilized to parameterize the accumulation mode volume size distributions of biomass burning and urban/industrial aerosols [*Remer et al.*, 1998; *Reid et al.*, 1998; *Remer and Kaufman*, 1998]. As noted previously (Figure 6), there is a tendency for increasing particle size as aerosol optical depth increases (Figure 9), with the peak in the distribution of the accumulation mode volume radius of the aerosol at KCO increasing from ~0.15 μm at τ_{a440} = 0.15 to ~0.20 μm at τ_{a440} = ~0.70. The coarse-mode particles (>0.6 μm), however, do

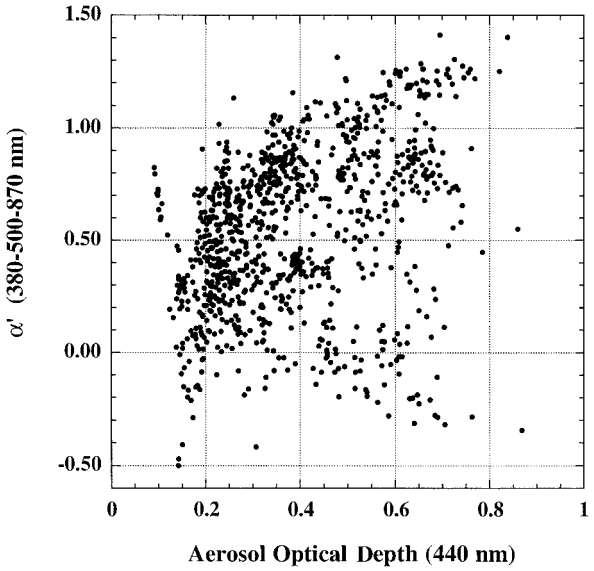

Figure 8. The value of α' ($d\alpha/d$ lnλ) computed from instantaneous τ_a values at 380, 500, and 870 nm at KCO for January–March 1999, as a function of aerosol optical depth at 440 nm.

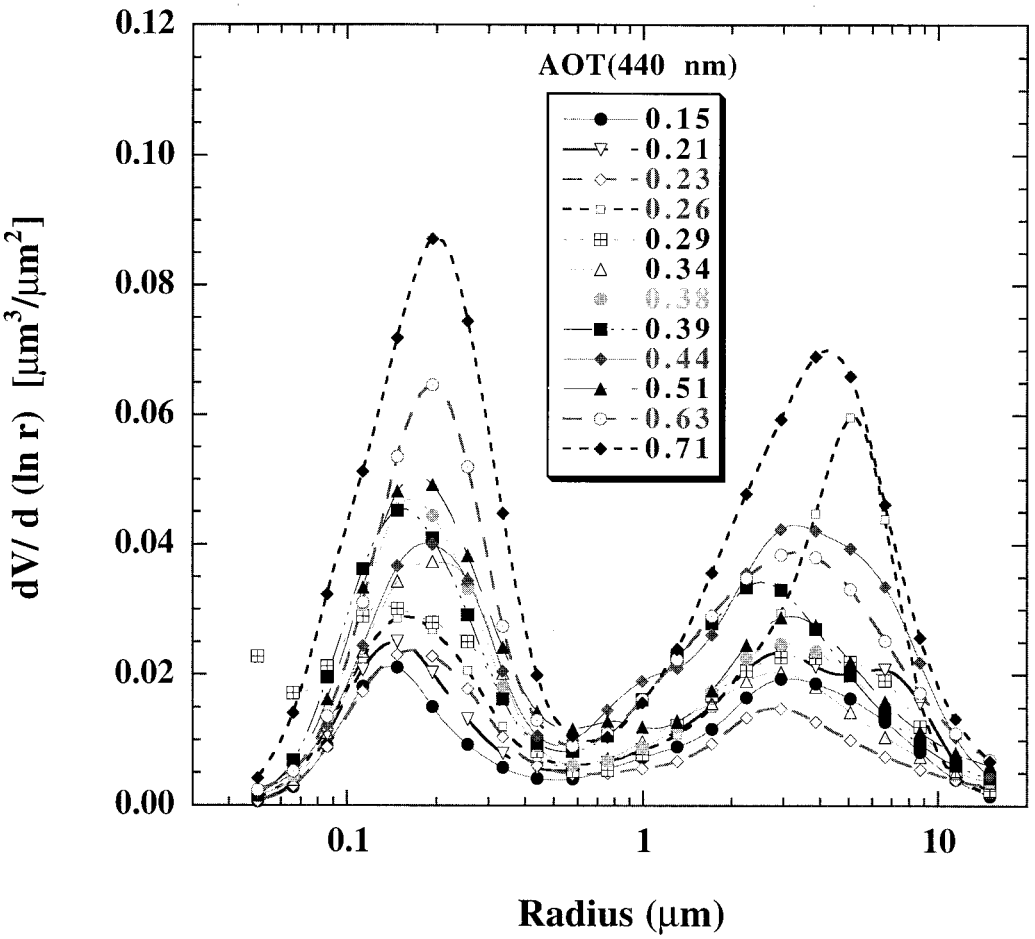

Figure 9. Aerosol volume size distributions at KCO for January–March 1999 for aerosol optical depth at 440 nm varying from 0.15 to 0.71. Aerosol size distribution retrievals were derived from simultaneous analysis of sky radiances in the almucantar and spectral τ_a at 440, 675, 870, and 1020 nm. Each size distribution is an average computed from six individual almucantar scan retrievals.

not show a clear trend in size as a function of aerosol optical depth. A preliminary comparison of in situ measured size distributions (provided by S. Howell, personal communication, 2001) at several altitudes from aircraft over the ocean NW of Male (~80 km from the CIMEL on Kaashidhoo) was done for 1 day, March 7, 1999. Some of the data corrections of the aircraft data were preliminary; however, the initial comparison between the size distributions for these two very different approaches showed bimodality for both data sets with both distributions also showing similar-sized particles for each of the modes.

As *Satheesh et al*. [1999] have discussed in detail, the aerosol size distributions at KCO are bimodal in nature. They identified several major components to the aerosol, which contribute in varying amounts to the total loading. The mixture of aerosol types present at KCO depends upon factors influencing the strengths of the aerosol sources, upon the trajectories of the air masses arriving at KCO (from different source regions), and on meteorological dispersion and scavenging mechanisms. The fine-mode aerosols observed at KCO are produced primarily as a result of anthropogenic combustion processes mainly from the use of fossil fuels [*Novakov et al*., 2000] with some biomass fuels and also various industrial processes. In addition, satellite-measured fire counts from landscape-level biomass burning reach a maximum over the Indian subcontinent in March [*Goloub and Arino*, 2000]. Industrial activity in conjunction with the petroleum industry in the Persian Gulf region also produces infrared emission signatures which are visible from satellite [*Goloub and Arino*, 2000], and emissions associated with this activity produce fine-mode aerosols which frequently occur in the Gulf region [*Smirnov et al*., 2001]. The coarse aerosol mode that we observe at KCO, results partly from combustion processes and also partly from entirely different processes and source regions. These aerosols have significant contributions from sea salt formed from ocean wave activity and from the long-distance transport of soil dust particles from desert and semiarid regions, such as the Arabian Peninsula and the Thar Desert in the Pakistan/India border region.

As we previously noted in section 3.1 (Figure 3), the lower values of the Angstrom wavelength exponent in January–March in the year 2000 as compared to 1999 suggest a larger relative contribution of coarse-mode particles in 2000. In Figure 10 we compare the size distributions retrieved from the CIMEL data for these 2 years, computed from averages of several almucantar scans for specific high values of aerosol optical depth. For 1999 the size distributions shown are averages computed from six individual scans for the months January–March, while for 2000 there were nine scans averaged for the months of January–April. The month of April was excluded from the 1999 averages due to the low Angstrom exponent for

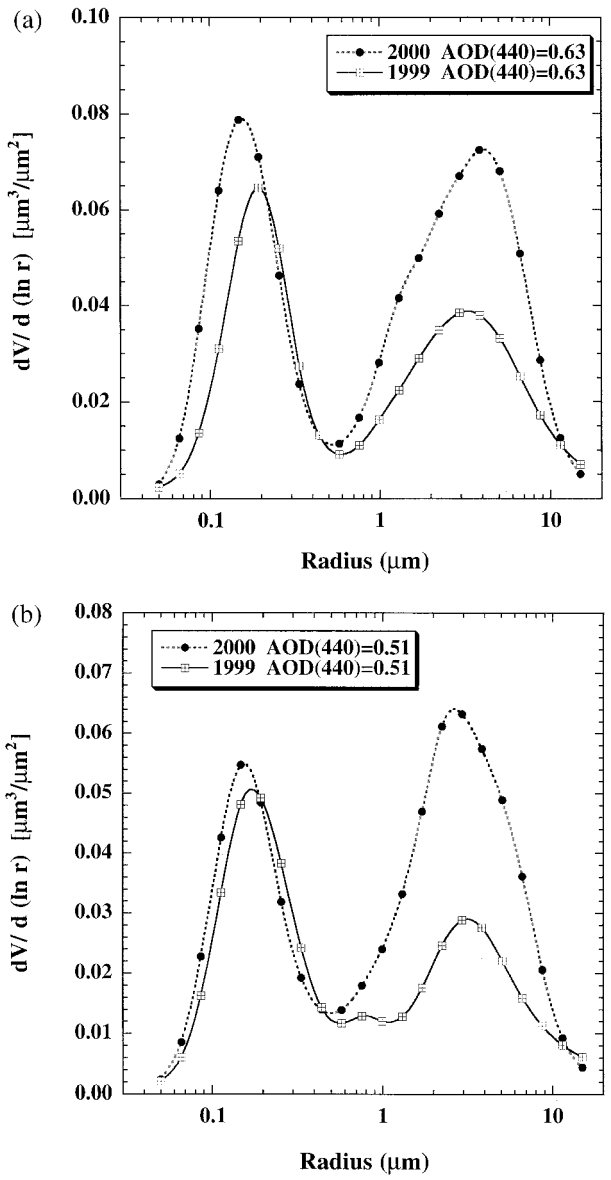

Figure 10. (a) Comparison of aerosol volume size distributions at KCO from January–March 1999 to those from January–April 2000 for aerosol optical depth at 440 nm averaging 0.63. (b) Same as in Figure 10a, but for aerosol optical depth at 440 nm of 0.51.

that month (Figure 3) as a result of trajectories predominately originating in Arabia in April 1999 [*Lobert and Harris*, this issue]. As expected from the Angstrom exponent analysis, the coarse-mode component of the volume size distribution is significantly larger in 2000 at both levels of optical depth shown ($\tau_{a500} = 0.63$ and 0.51) in Figure 10. These differences in the magnitude of the coarse-mode size distribution amplitude between the years 1999 and 2000 significantly exceed the retrieval uncertainty (~25% for particle radius >0.1 μm and <7 μm) which result from various instrumental offsets [*Dubovik et al.*, 2000]. In addition to the significantly higher coarse-mode component in 2000, the fine-mode aerosols in 2000 were shifted to a smaller size, from ~0.175–0.195 μm in 1999 to ~0.150 μm in 2000. It is noted that in the year 2000 the NE monsoon season was one of extreme drought in India, which may possibly have resulted in soil moisture conditions conducive to additional contributions of soil dust aerosols from arid regions in the subcontinent.

The scattering phase function of the aerosols was obtained from Mie calculations utilizing the retrieved volume size distributions and refractive indices from the almucantar sky radiances and spectral aerosol optical depth data. These phase function retrievals were used to compute the asymmetry factor g, which is the average cosine of the scattering direction weighted by the phase function, and which equals 1 for pure forward scattering and -1 for complete backscattering. Characterization of the aerosol scattering phase function at KCO is important since a lack of measurements at KCO of this parameter was identified as a likely source of error which may account for the systematic discrepancy found between measured and calculated diffuse fluxes by *Podgorny et al.* [2000]. Table 1 shows values of the real and imaginary parts of the refractive indices and asymmetry parameter at 440, 675, 870, and 1020 nm averaged for all observations where $\tau_{a440} > 0.40$ for the January–March 1999 time period. The real part of the refractive index shows little spectral dependence ranging from 1.42 to 1.46, and these are column-integrated radiatively effective values which involve the influences of both the fine and coarse modes. The average asymmetry factor (where $\tau_{a440} > 0.40$) representative of the total aerosol layer exhibits a distinct wavelength dependence with $g = 0.74$ at 440 nm and decreasing to 0.61 at 1020 nm (Table 1). A comparison of the spectral asymmetry parameter at high optical depths between the years 1999 and 2000 is given in Figure 11 for the same set of observations as was shown in Figure 10. There is relatively

Table 1. January–March 1999 Averages and Standard Deviations for AOD (440 nm) >0.4

	440 nm	670 nm	870 nm	1020 nm
SSA, ω_o				
average	0.91	0.88	0.84	0.83
s.d.	0.024	0.035	0.050	0.058
REFI real				
average	1.42	1.44	1.44	1.46
s.d.	0.060	0.045	0.037	0.036
REFI imaginary				
average	0.012	0.014	0.017	0.019
s.d.	0.005	0.007	0.009	0.011
Asymmetry, g				
average	0.74	0.67	0.63	0.61
s.d.	0.025	0.026	0.027	0.028

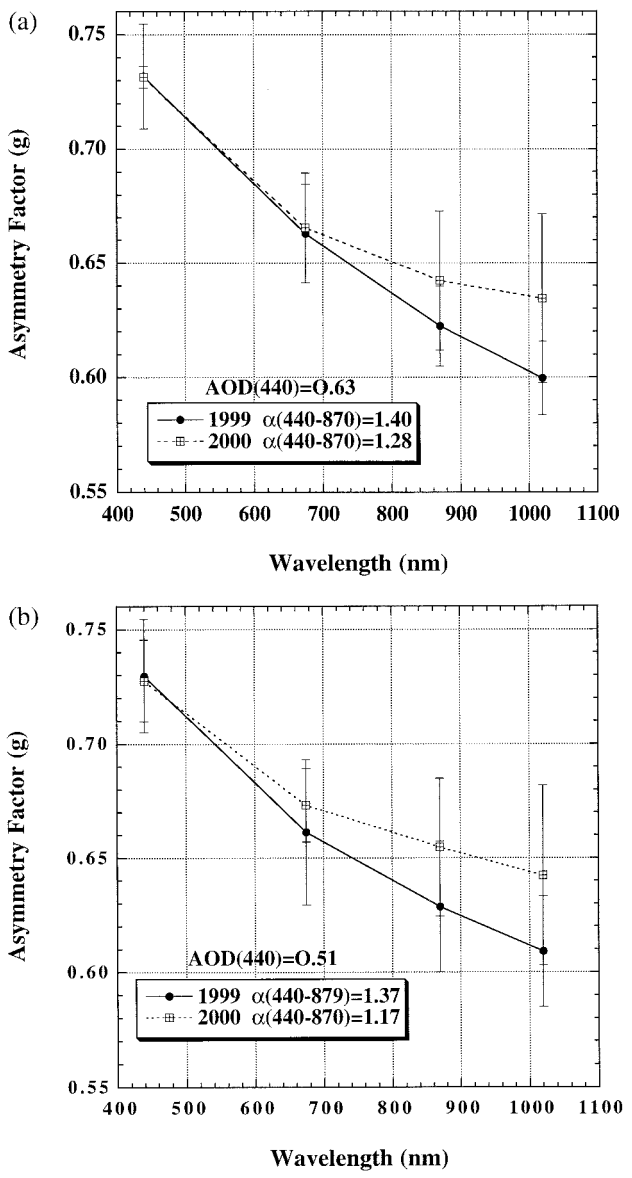

Figure 11. (a) Comparison of spectral asymmetry factors at KCO from January–March 1999 to those from January–April 2000 for aerosol optical depth at 440 nm averaging 0.63. Error bars show one standard deviation of the individual retrievals for six retrievals in 1999 and nine retrievals in 2000. (b) Same as in Figure 11a, but for aerosol optical depth at 440 nm of 0.51.

little variation in g between these years at the shorter wavelengths (440 and 675 nm), while g was larger in the year 2000 at 870 and 1020 nm. The greater relative contribution of coarse mode particles to the aerosol size distribution in 2000 therefore resulted in a phase function shift toward greater forward scattering at the longer (infrared) wavelengths, and very little change in the short (visible) wavelengths.

3.3. Single Scattering Albedo

The relatively strong absorption properties of the aerosols observed at KCO, coupled with high optical depths, result in large reductions in global irradiance at the ocean surface in both the total shortwave spectrum [*Satheesh et al*., 1999] and the photosynthetically active radiation (PAR) spectral region [*Conant*, 2000; *Podgorny et al*., 2000]. This strong aerosol absorption in the Maldives is due to the presence of soot (primarily from fossil fuel combustion and biomass burning), which *Satheesh et al*. [1999] have determined contributes ~11% to the midvisible aerosol optical depth (τ_{a500}). The soot component of the total aerosol is responsible for the clear-sky solar radiative heating during the NE monsoon being significantly decreased at the ocean surface, but decreased by a factor of 3 less at the top of the atmosphere [*Satheesh and Ramanathan*, 2000].

Several independent techniques were utilized during the INDOEX experiment to estimate the aerosol single scattering albedo ω_o, utilizing both in situ and remote sensing techniques based on measurements made from the land, ships, and aircraft. Estimates were made in situ from both the surface and from aircraft utilizing nephelometers and particle/soot absorption photometry. Lidar measurements were taken at Hulule island (~80 km south of KCO) and utilized to estimate vertical profiles of single scattering albedo [*Müller et al*., 2000]. In addition, simulation of solar radiation fluxes, with measured spectral τ_a as one of the inputs, in conjunction with measured fluxes was employed to retrieve estimates of ω_o [*Satheesh et al*., 1999]. Comparison of retrievals from all of these techniques with the addition of the CIMEL instrument retrieval [*Dubovik and King*, 2000] was presented by *Ramanathan et al*. [this issue]. The ω_o values estimated for 530 nm obtained by these diverse methods for the NE monsoon time period in the Maldives region ranged from averages of ~0.85 to 0.90 for surface in situ techniques, and ~0.86 to 0.90 for column averages. The retrievals we made at KCO with the CIMEL measurements averaged 0.90 at this wavelength. The ω_o estimates made from surface measurements at KCO and from the research vessel *Ronald H. Brown* in the Arabian Sea and Bay of Bengal ranged from averages of ~0.86–0.88 for the 1999 intensive field phase of INDOEX [*Ramanathan et al*., this issue]. These values show good agreement within the uncertainty levels of the AERONET and in situ retrievals; however, further study is warranted to investigate the differences in absorption obtained from the different techniques and to better quantify the altitude profile of ω_o. More information regarding comparisons of ω_o retrievals from different techniques and sites and the relative uniformity of ω_o values obtained over the Northern Hemisphere INDOEX study region is given by *Ramanathan et al*. [this issue].

However, there have not yet been any reported retrievals or calculations of the spectral dependence of ω_o for the INDOEX region during the NE monsoon. Single scattering albedo retrievals obtained from the CIMEL measurements at KCO at 440, 675, 870, and 1020 nm are presented in Figure 12, as a function of τ_{a440}. Each point shown in Figure 12 is a mean computed from retrievals of six individual almucantar scans, and the uncertainty in the individual ω_o retrievals is ~0.03 for $\tau_{a440} > 0.5$ with larger uncertainty for lower aerosol optical depths [*Dubovik et al*., 2000]. Higher ω_o retrieval uncertainty at low optical depth may possibly result in values that are not consistent with the aerosol physical and/or chemical properties, even though the impact of larger uncertainty in ω_o is less at low values of aerosol optical depth. In Figure 12, significant wavelength dependence of the single scattering albedo is noted, with ω_o decreasing as wavelength increases. Similarly, significant spectral variation of single scattering albedo in the visible and near-infrared has been inferred for biomass burning aerosols, urban/industrial aerosols, and desert dust [*Eck et al*.,

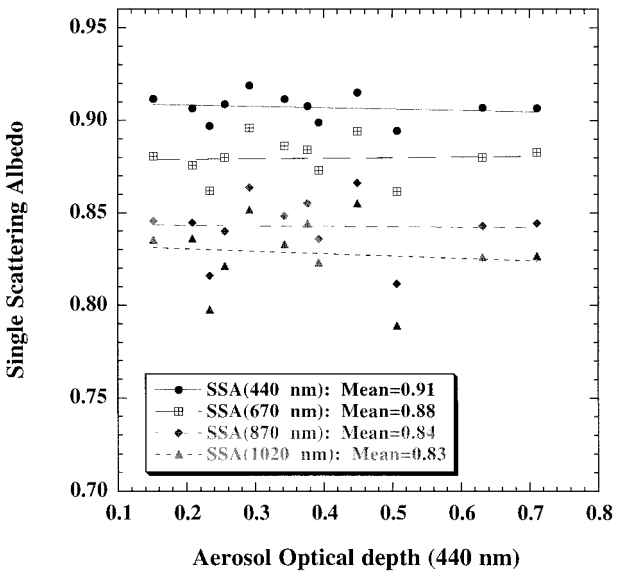

Figure 12. Retrievals of spectral ω_o from CIMEL instrument Sun and sky radiances and the algorithm of *Dubovik and King* [2000] for January–March 1999 at KCO. Each point on the graph is an average computed from six individual almucantar scan retrievals.

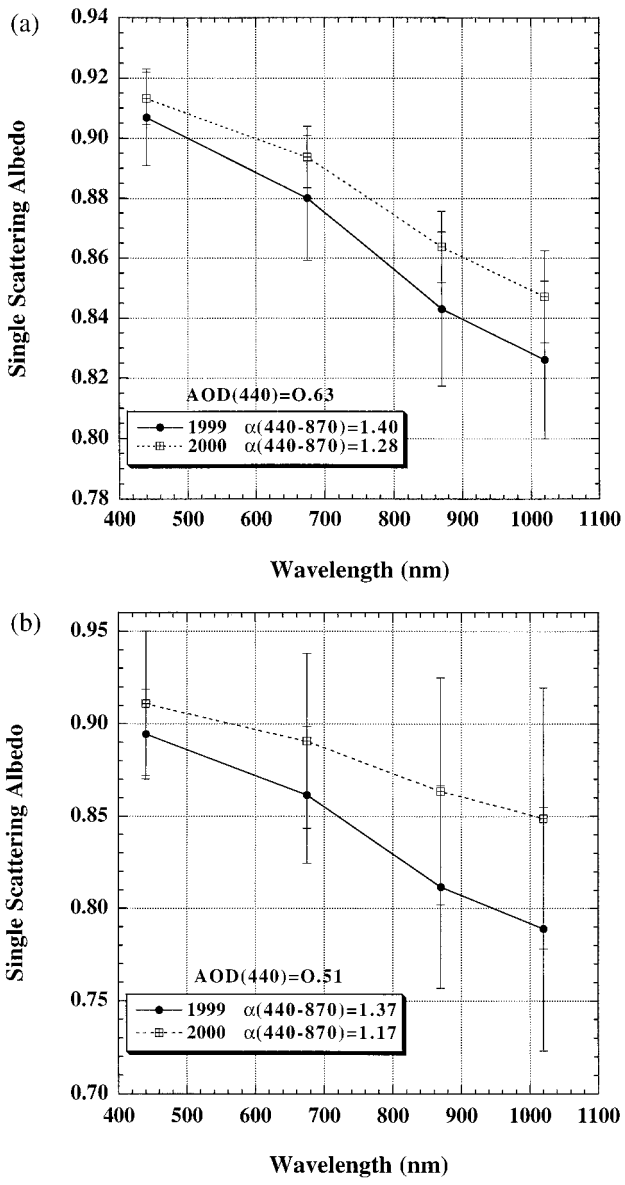

Figure 13. (a) Comparison of spectral single scattering albedo at KCO from January–March 1999 to those from January–April 2000 for aerosol optical depth at 440 nm averaging 0.63. Error bars show one standard deviation of the individual retrievals for six retrievals in 1999 and nine retrievals in 2000. (b) Same as in Figure 13a, but for aerosol optical depth at 440 nm of 0.51.

1998, 2001; *Dubovik et al*., 2001]. *Dubovik et al*. [2001] have shown from retrievals utilizing the same algorithm and identical CIMEL instruments from AERONET network sites that ω_o typically decreases with increasing wavelength for both biomass burning aerosols and for some urban regions. Specifically, the magnitude of ω_o at all wavelengths for KCO was similar (within ~0.015) to that observed in Mexico City (one of the world's largest urban centers) and for biomass burning aerosols in South American cerrado (savanna) regions, for an aerosol loading of $\tau_{a440} = 0.7$ at all three sites. In comparison, the ω_o at all wavelengths at KCO was higher than observed for African savanna burning aerosols in Zambia and lower than for biomass burning aerosols in Amazonian forested/pasture regions [*Dubovik et al*., 2001]. The large range in ω_o for biomass burning aerosols from different regions is due in large part to differences in fuel type and fuel moisture levels, which are significant factors governing what percentage of the total combustion is in the flaming versus smoldering phases. The resultant aerosols produced from the flaming phase of combustion of biomass fuels have higher black carbon content than are produced in the smoldering phase [*Ward et al*., 1992, 1996]. The regional hazes which result have lower ω_o for regions such as Zambia, where there is more flaming phase combustion [*Eck et al*., 2001].

The interannual variability of spectral single scattering albedo at KCO was also investigated. Owing to the low aerosol optical depths in 1998, we do not present ω_o retrievals for that year due to the relatively large uncertainty in the retrievals. We focus on the observations with high optical depths in 1999 and 2000, where $\tau_{a440} > 0.5$ and the resulting uncertainty in retrieved ω_o is ~0.03 [*Dubovik et al*., 2000]. The spectral values shown in Figure 13 are the means computed from six almucantar scans in 1999 and nine scans in 2000, with one standard deviation error bars also shown. For both levels of aerosol optical depth presented, $\tau_{a440} = 0.51$ and 0.63, the ω_o at all wavelengths is greater in 2000 than in 1999. The differences between 1999 and 2000 at $\tau_{a440} = 0.63$ are within the uncertainty level of the retrievals, while for $\tau_{a440} = 0.51$ the differences in the near-infrared wavelengths are as large as 0.06 which are beyond the differences expected by the uncertainty of the retrieval. It is noted that the Angstrom wavelength exponents are higher in 1999 than 2000 and that the difference in α (computed from linear regression of the 440, 675, 870, and 1020 nm τ_a) is 0.12 at $\tau_{a440} = 0.63$ and 0.20 at $\tau_{a440} = 0.51$ (Figure 13). Thus the lower α value in 2000 at $\tau_{a440} = 0.51$ implies a relatively greater coarse-mode contribution to the total aerosol in 2000, associated with the higher ω_o values, particularly at the longer wavelengths. The spectral ω_o of desert dust aerosols in central Saudi Arabia retrieved from CIMEL measurements [*Dubovik et al*., 2001] is very high at 870

and 1020 nm, ~0.97, and decreases to ~0.92 at 440 nm. Thus the higher ω_o especially at the longer wavelengths in 2000 versus 1999 is consistent with a possible increased contribution of desert dust aerosols to the total loading in 2000.

For the $\tau_{a440} = 0.51$ cases, since α is lower in 2000, the aerosol optical depth at 1020 nm will be higher than in 1999 for the same value of τ_a at 440 nm. However, at the same time, the lower ω_o values in 2000 will partly offset the higher infrared wavelength optical depth in the effects of aerosol attenuation of spectral surface irradiance in the near-infrared but also decrease the aerosol layer heating attributed to the near-infrared spectral region due to decreased absorption. Differences in the radiative effects of different aerosol composition in these 2 years at a given τ_{a440} level will be less pronounced in the PAR (400–700 nm) region due to smaller interannual differences of ω_o at these wavelengths, and also smaller differences of spectral τ_a, than for the near-infrared wavelengths. Modeling simulation analysis of the difference in the radiative effects of these interannual changes in aerosol composition for the ocean surface, the aerosol layer, and the top of the atmosphere needs to be carried out in order to better understand the effects of these aerosols on the regional climate.

4. Summary and Conclusions

Measurements of spectral aerosol optical depth and directional sky radiances were made with AERONET Sun-sky radiometers in Kaashidhoo, Republic of Maldives, from 1998–2000 to characterize the aerosol optical properties and their interannual variability for these years. The principal findings of our analysis of data from the NE monsoon months are summarized as follows:

1. Large interannual variability of aerosol optical depth was observed over the Kaashidhoo Climate Observatory during the NE monsoon months of January through April 1998, 1999, and 2000. For example, the monthly averages of τ_{a500} in February–April 1999 were approximately twice as high or greater as were observed in 1998, with the year 2000 being intermediate in magnitude.

2. Spectral variation of τ_a as parameterized by the Angstrom wavelength exponent also exhibited interannual variability, with lower monthly average values of α in 2000 compared to 1999 for the months of January–March. This is the result of a relatively greater contribution of coarse-mode particles (radius >0.6 μm) to total optical depth in 2000, possibly as a result of greater source strength for coarse particles in 2000 and/or increased transport from arid or semiarid regions to KCO. In addition, the relationship of ln τ_a versus ln λ showed significant departures from linearity especially for cases with high τ_a and where the fine mode had a greater relative influence.

3. Aerosol size distribution retrievals at KCO show persistent bimodality, and significant interannual variations in 1999 and 2000. In addition to greater relative amplitude of coarse-mode particles in 2000 relative to 1999, the size of the fine-mode particles also differed for these years, with fine-mode peak radius ~0.20 μm in 1999 versus ~0.15 μm in 2000, for high aerosol optical depth cases ($\tau_{a500} > 0.50$). The scattering phase function and the asymmetry factor, which are primarily governed by the size distribution, also showed interannual variation for these years. The magnitude of g is greater in 2000 in the infrared wavelengths (870 and 1020 nm), but remains nearly constant for both years in the visible wavelengths (440 and 675 nm).

4. The retrieved aerosol single scattering albedo observed at Kaashidhoo exhibited nearly linear wavelength dependence, ranging from $\omega_o \sim 0.91$ at 440 nm to $\omega_o \sim 0.83$ at 1020 nm (January–March 1999 averages where $\tau_{a440} > 0.40$). These relatively low ω_o values result from the significant contribution of soot to the total optical depth [*Satheesh et al*., 1999]. Some interannual variability in spectral ω_o was also observed, with higher values in 2000 than 1999, especially in the infrared wavelengths. Greater contribution of desert dust aerosols to the total optical depth in 2000 may explain this interannual spectral change in ω_o, as AERONET retrievals of ω_o for desert dust in central Saudi Arabia show relatively high ω_o (~0.97) at 870 and 1020 nm, yet low values (<0.92) at 440 nm [*Dubovik et al*., 2001].

Thus our analysis suggests that in addition to significant interannual variations in concentrations of aerosols in the Maldives that occurred for the 1998–2000 NE monsoon seasons, the optical properties of the aerosols may also have varied at times for these years. Continued monitoring of the aerosol optical properties in the region is needed in order to better understand the magnitude and causes of this variability, and also to detect any possible long-term trends in aerosol loading and/or optical properties. NASA's AERONET project is planning on continuing monitoring in the Maldives and adjacent continental regions, such as in Saudi Arabia, and also has recently established a site on the Indian subcontinent.

Acknowledgments. This project was supported by Mike King, EOS Project Office. We acknowledge the critical efforts of AERONET team members Nader Abuhassen, Wayne Newcomb, and Adam Naji in maintaining and adjusting the radiometers deployed in the AERONET network. Rangasayi Halthore provided the results of the LBL-RTM simulations to determine the water vapor optical depths at 1020 nm. We also thank Asif Ali and Azim Abdulraheem at the Kaashidhoo Climate Observatory for maintenance of the CIMEL radiometers located there.

References

Ackerman, A. S., O. B. Toon, D. E. Stevens, A. J. Heymsfield, V. Ramanathan, and E. J. Welton, Reduction of tropical cloudiness by soot, *Science*, *288*, 1042–1047, 2000.

Bruegge, C. T., J. E. Conel, R. O. Green, J. S. Margolis, R. G. Holm, and G. Toon, Water vapor column abundance retrievals during FIFE, *J. Geophys. Res*., *97*, 18,759–18,768, 1992.

Clough, S. A., M. J. Iacono, and J.-L. Moncet, Line-by line calculation of atmospheric fluxes and cooling rates: Application to water vapor, *J. Geophys. Res*., *97*, 15,761–15,785, 1992.

Conant, W. C., An observational approach for determining aerosol surface radiative forcing: Results from the first field phase of INDOEX, *J. Geophys. Res*., *105*, 15,347–15,360, 2000.

Dubovik, O., and M. D. King, A flexible inversion algorithm for the retrieval of aerosol optical properties from Sun and sky radiance measurements, *J. Geophys. Res*., *105*, 20,673–20,696, 2000.

Dubovik, O., A. Smirnov, B. N. Holben, M. D. King, Y. J. Kaufman, T. F. Eck, and I. Slutsker, Accuracy assessments of aerosol optical properties retrieved from AERONET Sun and sky-radiance measurements, *J. Geophys. Res*., *105*, 9791–9806, 2000.

Dubovik, O., B. N. Holben, T. F. Eck, A. Smirnov, Y. J. Kaufman, M. D. King, D. Tanre, and I. Slutsker, Variability of absorption and optical properties of key aerosol types observed in worldwide locations, *J. Atmos. Sci*., in press, 2001.

Eck, T. F., B. N. Holben, I. Slutsker, and A. Setzer, Measurements of irradiance attenuation and estimation of aerosol single scattering albedo for biomass burning aerosols in Amazonia, *J. Geophys. Res*., *103*, 31,865–31,878, 1998.

Eck, T. F., B. N. Holben, J. S. Reid, O. Dubovik, A. Smirnov, N. T.

O'Neill, I. Slutsker, and S. Kinne, Wavelength dependence of the optical depth of biomass burning, urban, and desert dust aerosols, *J. Geophys. Res*., *104*, 31,333–31,349, 1999.

Eck, T. F., B. N. Holben, D. E. Ward, O. Dubovik, J. S. Reid, A. Smirnov, M. M. Mukelabai, N. C. Hsu, N. T. O'Neill, and I. Slutsker, Characterization of the optical properties of biomass burning aerosols in Zambia during the 1997 ZIBBEE field campaign, *J. Geophys. Res*., *106*, 3425–3448, 2001.

Giver, L. P., C. Chackerian Jr., and P. Varanasi, Visible near-infrared H_2O line intensity corrections for HITRAN96, *J. Quant. Spectrosc. Radiat. Transfer*, *66*, 101–105, 2000.

Goloub, P., and O. Arino, Verification of the consistency of POLDER Aerosol Index over land with ATSR-2 fire product, *Geophys. Res. Lett*., *27*, 899–902, 2000.

Hansen, J., M. Sato, and R. Ruedy, Radiative forcing and climate response, *J. Geophys. Res*., *102*, 6831–6864, 1997.

Hansen, J., M. Sato, R. Ruedy, A. Lacis, and V. Oinas, Global warming in the twenty-first century: An alternative scenario, *Proc. Natl. Acad. Sci. U. S. A*., *97*, 9875–9880, 2000.

Holben, B. N., et al., AERONET—A federated instrument network and data archive for aerosol characterization, *Remote Sens. Environ*., *66*, 1–16, 1998.

Holben, B. N., et al., An emerging ground-based aerosol climatology: Aerosol optical depth from AERONET, *J. Geophys. Res*., *106*, 12,067–12,097, 2001.

King, M. D., Y. J. Kaufman, D. Tanre, and T. Nakajima, Remote sensing of tropospheric aerosols from space: Past, present, and future, *Bull. Am. Meteorol. Soc*., *80*, 2229–2259, 1999.

Lobert, J. M., and J. M. Harris, Trace gases and air mass origin at Kaashidhoo, Indian Ocean, *J. Geophys. Res*., this issue.

Martins, J. V., P. V. Hobbs, R. E. Weiss, and P. Artaxo, Sphericity and morphology of smoke particles from biomass burning in Brazil, *J. Geophys. Res*., *103*, 32,051–32,057, 1998.

Müller, D., F. Wagner, D. Althausen, U. Wandinger, and A. Ansmann, Physical properties of the Indian aerosol plume derived from six-wavelength lidar observations on 25 March 1999 of the Indian Ocean Experiment, *Geophys. Res. Lett*., *27*, 1403–1406, 2000.

Novakov, T., M. O. Andreae, R. Gabriel, T. W. Kirchstetter, O. L. Mayol-Bracero, and V. Ramanathan, Origin of carbonaceous aerosols over the tropical Indian Ocean: Biomass burning or fossil fuels?, *Geophys. Res. Lett*., *27*, 4061–4064, 2000.

O'Neill, N. T., T. F. Eck, B. N. Holben, A. Smirnov, O. Dubovik, and A. Royer, Bimodal size distribution influences on the variation of Angstrom derivatives in spectral and optical depth space, *J. Geophys. Res*., *106*, 9787–9806, 2001.

Podgorny, I. A., W. Conant, V. Ramanathan, and S. K. Satheesh, Aerosol modulation of atmospheric and surface solar heating over the tropical Indian Ocean, *Tellus*, *Ser. B*, *52*, 947–958, 2000.

Rajeev, K., V. Ramanathan, and J. Meywerk, Regional aerosol distribution and its long-range transport over the Indian Ocean, *J. Geophys. Res*., *105*, 2029–2043, 2000.

Ramanathan, V., et al., Indian Ocean Experiment: An integrated analysis of the climate forcing and effects of the great Indo-Asian haze, *J. Geophys. Res*., this issue.

Reid, J. S., P. V. Hobbs, R. J. Ferek, D. R. Blake, J. V. Martrins, M. R. Dunlap, and C. Liousse, Physical, chemical, and optical properties of regional hazes dominated by smoke in Brazil, *J. Geophys. Res*., *103*, 32,059–32,080, 1998.

Reid, J. S., T. F. Eck, S. A. Christopher, P. V. Hobbs, and B. N. Holben, Use of the Angstrom exponent to estimate the variability of optical and physical properties of aging smoke particles in Brazil, *J. Geophys. Res*., *104*, 27,473–27,489, 1999.

Remer, L. A., and Y. J. Kaufman, Dynamic aerosol model: Urban/industrial aerosol, *J. Geophys. Res*., *103*, 13,859–13,871, 1998.

Remer, L. A., Y. Kaufman, B. N. Holben, A. M. Thompson, and D. P. McNamara, Biomass burning aerosol size distribution and modeled optical properties, *J. Geophys. Res*., *103*, 31,879–31,891, 1998.

Satheesh, S. K., and V. Ramanathan, Large differences in tropical aerosol forcing at the top of the atmosphere and Earth's surface, *Nature*, *405*, 60–63, 2000.

Satheesh, S. K., V. Ramanathan, X. Li-Jones, J. M. Lobert, I. A. Podgorny, J. M. Prospero, B. N. Holben, and N. G. Loeb, A model for the natural and anthropogenic aerosols over the tropical Indian Ocean derived from Indian Ocean Experiment data, *J. Geophys. Res*., *104*, 27,421–27,440, 1999.

Schmid, B., J. Michalsky, R. Halthore, M. Beauharnois, L. Harrison, J. Livingston, P. Russell, B. Holben, T. Eck, and A. Smirnov, Comparison of aerosol optical depth from four solar radiometers during the fall 1997 ARM intensive observation period, *Geophys. Res. Lett*., *26*, 2725–2728, 1999.

Shaw, G. E., Absorption continuum in the near IR near 1 μm, *Appl. Opt*., *19*, 480–482, 1980.

Smirnov, A., B. N. Holben, T. F. Eck, O. Dubovik, and I. Slutsker, Cloud screening and quality control algorithms for the AERONET database, *Remote Sens. Environ*., *73*, 337–349, 2000.

Smirnov, A., B. N. Holben, O. Dubovik, D. L. Westphal, A. K. Goroch, C. R. McClain, T. F. Eck, and I. Slutsker, Atmospheric aerosol optical properties in the Persian Gulf region, *J. Atmos. Sci*., in press, 2001.

Ward, D. E., R. A. Susott, J. B. Kaufman, R. E. Babbitt, D. L. Cummings, B. Dias, B. N. Holben, Y. J. Kaufman, R. A. Rasmussen, and A. W. Setzer, Smoke and fire characteristics for cerrado and deforestation burns in Brazil: Base-B experiment, *J. Geophys. Res*., *97*, 14,601–14,619, 1992.

Ward, D. E., W. M. Hao, R. A. Susott, R. E. Babbitt, R. W. Shea, J. B. Kaufman, and C. O. Justice, Effect of fuel composition on combustion efficiency and emission factors for African savanna ecosystems, *J. Geophys. Res*., *101*, 23,569–23,576, 1996.

O. Dubovik, T. F. Eck, B. N. Holben, I. Slutsker, and A. Smirnov, NASA Goddard Space Flight Center, Mail Code 923, Greenbelt, MD 20771, USA. (tom@aeronet.gsfc.nasa.gov)

J. M. Lobert and V. Ramanathan, Center for Clouds, Chemistry, and Climate, Scripps Institution of Oceanography, University of California, San Diego, La Jolla, CA 92037, USA.

(Received October 19, 2000; revised February 16, 2001;
accepted April 18, 2001.)